Phase stabilities at a glance: Stability diagrams of nickel dipnictides

F. Bachhuber, J. Rothballer, T. Söhnel, and R. Weihrich

Citation: The Journal of Chemical Physics **139**, 214705 (2013); doi: 10.1063/1.4832698
View online: http://dx.doi.org/10.1063/1.4832698
View Table of Contents: http://scitation.aip.org/content/aip/journal/jcp/139/21?ver=pdfcov
Published by the AIP Publishing

Phase stabilities at a glance: Stability diagrams of nickel dipnictides

F. Bachhuber,[1,2] J. Rothballer,[1] T. Söhnel,[2,3] and R. Weihrich[1,a)]
[1]*University of Regensburg, Institute of Inorganic Chemistry, Universitätsstr. 31, 93040 Regensburg, Germany*
[2]*School of Chemical Sciences, The University of Auckland, Private Bag 92019, Auckland, New Zealand*
[3]*Centre for Theoretical Chemistry and Physics, The New Zealand Institute for Advanced Study, Massey University Auckland, Auckland, New Zealand*

(Received 4 July 2013; accepted 7 November 2013; published online 4 December 2013)

In the course of the recent advances in chemical structure prediction, a straightforward type of diagram to evaluate phase stabilities is presented based on an expedient example. Crystal structures and energetic stabilities of dipnictides NiPn_2 (Pn = N, P, As, Sb, Bi) are systematically investigated by first principles calculations within the framework of density functional theory using the generalized gradient approximation to treat exchange and correlation. These dipnictides show remarkable polymorphism that is not yet understood systematically and offers room for the discovery of new phases. Relationships between the concerned structures including the marcasite, the pyrite, the arsenopyrite/$CoSb_2$, and the $NiAs_2$ types are highlighted by means of common structural fragments. Electronic stabilities of experimentally known and related AB_2 structure types are presented graphically in so-called stability diagrams. Additionally, competing binary phases are taken into consideration in the diagrams to evaluate the stabilities of the title compounds with respect to decomposition. The main purpose of the stability diagrams is the introduction of an image that enables the estimation of phase stabilities at a single glance. Beyond that, some of the energetically favored structure types can be identified as potential new phases. © *2013 AIP Publishing LLC*. [http://dx.doi.org/10.1063/1.4832698]

I. INTRODUCTION

One of the greatest challenges in modern-day solid state chemistry is the search for novel functional materials as key compounds for high technological applications, e.g., to gain energy in thermoelectric or photovoltaic compounds.[1,2] On the way from expensive experimental screening to the prediction and finally to the design of materials, first-principles calculations play an increasingly important role not only to calculate properties of already synthesized compounds but also to predict the stabilities of hypothetical new compounds. The latter is significantly more complex and time-consuming and can be gradually more afforded with high-performance computers and advanced codes. As a result, the focus has been turned from the pure description of experimentally known compounds to the discovery of new materials by means of theoretical methods. A milestone to predict hitherto unknown compounds and structures was set by the work of Jansen,[3] emphasizing the role of theoretical methods in solid state chemistry synthesis planning. The introduction of the concept of an energy landscape that reflects the energy hypersurface of the material world and the exploration of this landscape delivers a key for rational design of syntheses. It is based on the principle that all possible structures and compositions are found on the potential energy surface that can be computed. Thereby, also metastable compounds can be identified. Another approach by Oganov *et al.* applies a combination of evolutionary techniques and *ab initio* calculations to predict stable and low-energy metastable structures.[4] Dronskowski *et al.* published a state-of-the-art contribution on *ab initio* thermochemistry of solid-state materials[5] and they developed energy–volume diagrams for systems with a fixed stoichiometry including a multitude of possible structure types.[6] The concept was applied by our group to calculate the relative stability of black and red phosphorus and arsenic.[7] A recent contribution by Zunger *et al.* dealing with stabilities of hypothetical *Half-Heusler*-type compounds emphasizes the role of competing phases with different atomic compositions in addition to thermodynamic stabilities.[8]

Keeping in mind the works cited above, we want to present a graphical representation using the example of an expedient and comprehensible case. It extends our earlier schemes that were based on the prediction of pyrite (FeS_2) related compounds.[9–15] In a systematic quantum mechanical study, relevant excerpts of the stated energy landscape are depicted for the example of nickel dipnictides. A well-established stepwise rough to precise optimization scheme starting from known nickel dipnictide and related structure types should provide a basis for the determination of reliable energy values. Applying this method, new structures or variations of those structures can also be detected. Competing binary phases with different stoichiometries are considered to provide an entire impression of the phase stabilities of the investigated series. Instead of a list of absolute energy values, a large-scale picture of relevant (hypothetical) phases is offered with emphasis on trends within the periodic table. Nickel dipnictides provide an ideal model system for this case study with the occurrence of several polymorphs on the one hand and enough room for the discovery of not-yet-known compounds on the other.

a)Author to whom correspondence should be addressed. Electronic mail: richard.weihrich@chemie.uni-r.de

Among the multitude of structure types known for several combinations of pnictides and transition metals, compounds with the stoichiometry MPn_2 (M = transition metal, Pn = pnictide) are very important representatives. With the exception of group 3 and group 7 elements, the formation of dipnictide compounds has been reported for all transition metals with at least one member of the pnictide row (according to the Inorganic Crystal Structure Database (ICSD)[16,17]). The structural diversity of the MPn_2 compounds ranges from layers, chains, and dumbbells to strand-like and spiral arrangements. Whereas layered structures are characteristic for earlier transition metals in MPn_2, later transition metals tend to prefer compounds containing dumbbells. The latter can be separated into 3 predominant structural groups: the marcasite type that mainly appears for group 8 elements, the arsenopyrite type that is characteristic for group 9 elements, and the pyrite type that is most common for group 10 elements. Pyrite (FeS_2) related compounds have been playing an important role in the development of theoretical calculations. Pyrite itself is under intensive investigation as it was identified as promising material for photovoltaic applications from band structure calculations.[18,19] Later, platinum nitride was identified as isoelectronic pyrite type PtN_2 by thorough density functional theory (DFT) calculations on possible stable compositions and structures.[20] It is isotypic and isoelectronic to pyrite and known compounds $PtPn_2$ (Pn = P, As, Sb, Bi) as well as SiP_2.[12,14] Furthermore, it exhibits an N-N bond similar to PdN_2, predicted ultrahard CN_2,[9,10] and large gap SiN_2.[10,12] Looking for isoelectronic $NiPn_2$ compounds, one finds a range of polymorphs and structurally related compounds that are known for possible applications as electrode materials.[21] Isoelectronic to FeS_2, $NiPn_2$-type compounds should reveal high oxidation potential as diamagnets with d^6 electronic configuration for Ni in a rather unusual oxidation state of +IV. The search for novel nickel dipnictides is expected to yield useful materials with interesting functionalities.

In contrast to the group 8 and group 9 metal dipnictides, there is a distinct structural diversity (beyond the pyrite type) among the group 10 metal dipnictides, particularly for M = Ni (Table I). In fact, the observed polymorphism for the nickel compounds is outstanding in the class of dipnictides. Nickel diarsenides exhibit the largest structural variety. $NiAs_2$ has a pararammelsbergite type[22–25] low temperature and a rammelsbergite/marcasite type[23,25–30] high temperature form while pyrite type $NiAs_2$[31,32] is found at high pressures. For $NiSb_2$, a marcasite type phase[33] was thoroughly studied by Kjekshus[25,28–30,34] and the application of high pressure was shown to lead to a pararammelsbergite type instead of a pyrite type structure.[35] NiP_2 crystallizes in a KO_2 type structure[36,37] at ambient conditions and a high temperature and high pressure form of NiP_2[32] exists in the pyrite type. The question arises if and how the mentioned structures are associated with each other and if some of the structure types could be found as new phases in combination with different pnictides. Not-yet-known pernitrides and dibismuthides are especially interesting in this matter as they have been reported for the corresponding palladium and platinum homologues.[38–47] Actually, the discovery of novel dinitride compounds was successful recently (OsN_2, IrN_2, PtN_2)[38–40,48] – driven by promising properties like hardness or superconductivity. This situation is seen as a starting point for the question on the prediction of the relative stability of known and unknown compounds and structures with respect to possible polymorphs and the decomposition into more stable products. Only a small number of quantum mechanical studies for nickel dipnictides have been performed to date: two works were dedicated to nickel diphosphides.[49,50] The $NiPn_2$ homologues $PdPn_2$ and especially $PtPn_2$, however, were in the focus of structure calculations mainly for Pn = N.[12,20,51–53] In this work, we want to investigate the stabilities of experimentally known and hypothetical structures of nickel dipnictides in the abovementioned and other related structure types and point out the relationships between the different structure types.

Stability diagrams serve as a basis for a classification of all known compounds within the examined series and guide the way to hitherto not existing materials. The main goal is to establish a reliable and straightforward way of identifying low-energy and lowest-energy crystal structures. The structure candidates are additionally related to the energies of their elements and competing binary Ni_xPn_y phases to evaluate their stabilities with respect to decomposition. Many hypothetical compounds are energetically stable with respect to decomposition into their elements but not into competing phases. The stability diagrams are meant to go beyond bare numbers and to get a bigger picture of the $NiPn_2$ systems that allows for an evaluation of phase stabilities at one glance. Optimized crystal structure data of the lowest-energy structures are compared to experimental data. A foundation for experimentalists should be provided to synthesize new materials with useful functionalities. Finally, tendencies within the pnictide row can be derived that allow for further understanding of bonding and other chemical trends within the group.

TABLE I. Overview of the existing crystal structures for nickel dipnictides.

$NiPn_2$	Ni	Pd	Pt
N			*Pa*-3 (205)
P	*Pa*-3 (205)[a]		*Pa*-3 (205)
	*C*2/*c* (15)[b]	*C*2/*c* (15)[b]	
As	*Pa*-3 (205)	*Pa*-3 (205)	*Pa*-3 (205)
	Pnnm (58)[a]		
	Pbca (61)[a]		
Sb	*Pnnm* (58)	*Pa*-3 (205)	*Pa*-3 (205)
	Pbca (61)[a]		
Bi		*C*2/*m* (12)[c]	*Pa*-3 (205)
		*I*4/*mmm* (139)[a]	*Pbca* (61)
			P-3 (147)[c]

[a]Dumbbell-like structures.
[b]Strand-like structures.
[c]Layered structures.

II. COMPUTATIONAL DETAILS

The first-principles electronic structure calculations were carried out within the framework of DFT with exchange-correlation functionals in the generalized gradient

approximation (GGA)[54,55] according to Perdew-Burke-Enzerhof (PBE). Full geometry optimizations were executed with the Vienna Ab initio Simulation Package (VASP);[56–59] atomic site parameters and cell constants were therefore allowed to fully relax with the conjugant gradient algorithm. The interactions between the ions and the electrons are described by the projector-augmented-wave (PAW) method[60,61] with a cutoff energy of 500 eV. All calculations were performed in three subsequent steps with an initial *k*-grid mesh of $4 \times 4 \times 4$ rising to $8 \times 8 \times 8$ and $12 \times 12 \times 12$ to reach sufficient accuracy. Particularly for large unit cells, this offers an additional verification of the performed calculations. A structure optimization was considered to be converged with a difference in total energy of less than 1×10^{-6} eV and a maximum Hellmann-Feynmann force of 1×10^{-4} eV/Å. The final values of the total energies of the investigated systems were obtained with energy differences (between last and second to last step) of less than 1×10^{-3} eV per formula unit. From additional calculations with initial spin polarization, no magnetic ground state and no energy gain could be observed for any of the systems.

III. CRYSTAL STRUCTURES

The experimental data of the structures shown in Table I deliver the basis for the starting crystal geometries. Along with the experimentally known Ni*Pn*$_2$ structures, the selection of investigated AB_2 structure types comprises corresponding Pd and Pt systems and adequate reference systems.

The structure types of the group 10 metal dipnictides can basically be divided into two groups, dumbbell-like and layered structures. The latter can be observed for palladium (monoclinic froodite, space group (SG) *C*2/*m* (12); tetragonal $CuZr_2$-type urvantsevite, SG *I*4/*mmm* (139)) and platinum (trigonal/rhombohedral $PtBi_2$, *P*-3 (147)) dibismuthide compounds. For all three structure types, *Pn-M-Pn* triple layers are stacked along one axis with increasing distortion from trigonal $PtBi_2$ to urvantsevite and froodite. They serve as potential structure candidates especially for $NiBi_2$. A more detailed description comparing and contrasting these and other layered structures will be published elsewhere. In addition, the related prototype structures cadmium iodide (CdI_2, SG *P*-3*m*1 (164)) and calcium fluoride (CaF_2, SG *Fm*-3*m* (225)) serve as further reference compounds for layered structures and structures with isolated ions.

The majority of the structure types under investigation, however, contain dumbbell-like arrangements. Structures of this and similar kind were subject to detailed investigations, particularly for homologous Pd and Pt compounds and the respective chalcogenides. Among these, there are the marcasite/rammelsbergite (orthorhombic, SG *Pnnm* (58)), the pyrite (cubic, SG *Pa*-3 (205)), the $NiAs_2$/pararammelsbergite (orthorhombic, SG *Pbca* (61)), the arsenopyrite/$CoSb_2$ (monoclinic, SG $P2_1/c$ (14)), and the KO_2 type (monoclinic, SG *C*2/*c* (15)) structure. By approximation, the latter can also be seen as dumbbell-like structure. Alternative to a chain-like description, dumbbells can be imagined as those that are interconnected as zigzag-like chains with almost equal distances within and between the pairs. Even though the mentioned dumbbell-like structures belong to different crystal systems and their unit cells differ in size and shape, they are all related to each other. A detailed discussion on the relationships between the pyrite, marcasite, and arsenopyrite type can be found in contributions by A. Kjekshus.[62–64] Many depictions of the unit cells found in the literature contain a rather unclear connection of coordination polyhedra or appear as mere congeries of the atoms of the unit cell. Here, we want to introduce a straightforward graphical representation with emphasis on common structural fragments to allow for a comparison of the present structure types.

The investigated structure types can all be derived from close-packed metal structures with dumbbells in octahedral holes. The main difference between the structures is the orientation of the dumbbells which can be seen in Figure 1 and will be explained below. This results in different symmetries, different space groups, and unit cells that significantly diverge in size and shape. Equivalent characteristic fragments can be found for all structure types with *Pn-Pn* dumbbells. *Pn* atoms are (distorted) tetrahedrally, coordinated by the corresponding dumbbell partner and 3 Ni atoms. An exception is the KO_2 type structure with two *Pn* neighbors and two Ni atoms. The Ni atoms exhibit a (distorted) octahedral coordination by *Pn* atoms except for the almost square planar coordination in the KO_2 type. The structural relationships can be well described based on the marcasite type. The structure images displayed in Figure 1 are characteristic fragments of the parent structures and do not represent their unit cells in a different setting. Dark lines symbolize the cell edges of a hypothetical marcasite-type unit cell and yellow lines represent the original unit cell edges. Atoms in the original unit cell that do not appear in the hypothetical marcasite type cell are shaded. The main diversities between the different structure types are the orientation and the displacement of the *Pn-Pn* entities and thus the connection of the coordination polyhedra and the divergence from the geometry of the marcasite unit cell. The following paragraph is devoted to a more detailed analysis of the relationships of the introduced structure types.

In marcasite, all dumbbells are located in parallel planes and they exhibit the same orientation in every second plane (0 0 2). The arsenopyrite structure is very similar to marcasite, solely the distances of the Ni atoms of every second plane alternately become shorter and larger. The *Pn-Pn* entities keep their orientations and are just slightly distorted compared to the marcasite structure. To get from the marcasite to the pyrite type structure, half of the *Pn-Pn* pairs are alternately turned perpendicular to the planes (in one direction of the plane only, they stay the same in the other direction) without changing their positions in M_6 octahedra. Accordingly, the planes are pushed apart and Ni-Ni distances in between become equidistant to the ones within the planes, i.e., the Ni atoms are arranged as an undistorted *fcc* type substructure with dumbbells in octahedral holes (cf. NaCl structure). Based on the marcasite type structure, the $NiAs_2$ type structure can approximately be obtained with a mixture of both transformations described above. Alternating *M-M* distances and orthogonally twisted dumbbells (in both directions of the plane) lead to a significantly distorted marcasite unit cell. To relate the KO_2 type to the marcasite type structure, all *Pn-Pn* entities are likewise

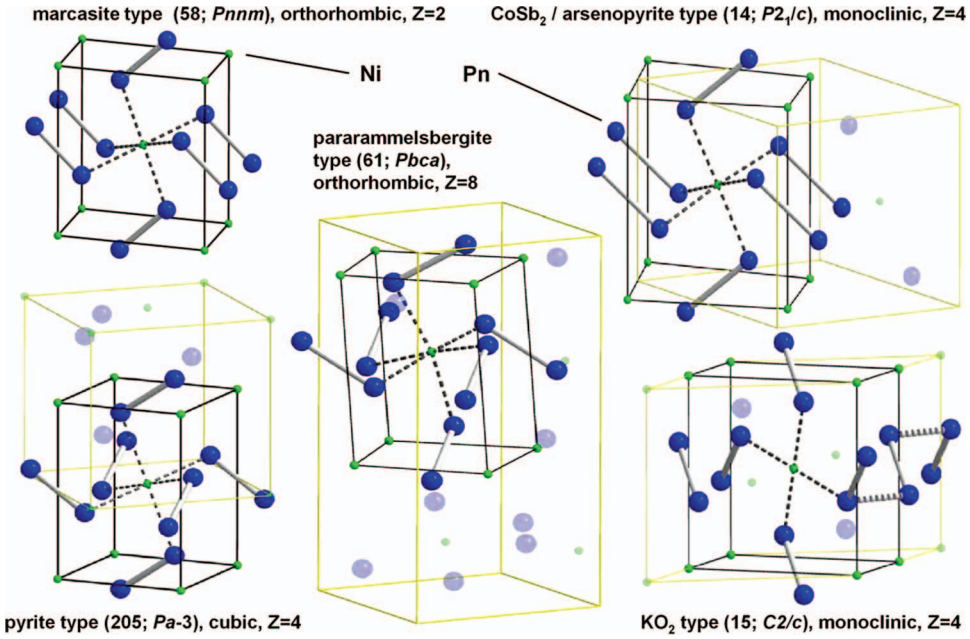

FIG. 1. Crystal structures of the dumbbell-like structure types. The structure fragments are based on the marcasite type and the original unit cells are indicated as yellow lines. The fragments are meant to indicate structural similarities and do not represent the unit cells in a different setting.

turned out of the plane in the same direction with alternately half of them rotated by another 180°. The Ni framework gets slightly distorted and the dumbbells are directed to each other in a way that zigzag-like chains are formed with almost identical distances between the *Pn* atoms. The (distorted) octahedral coordination of M atoms by *Pn* atoms is replaced by an almost square planar coordination and the (distorted) tetrahedrons around *Pn* atoms consist of 2 *Pn* and 2 *M* neighbors.

Summing up, the basic constitution of the examined structure types is very similar. Most distinctive deviations exist for the KO_2 type, and the arsenopyrite/$CoSb_2$ type is the only one that has not been reported for Ni/Pd/Pt dipnictides. It will be interesting to see if the described similarities can also be observed in the calculated stability diagrams in terms of energies and volumes and how they are affected by pnictide substitution. It is furthermore noteworthy that the KO_2 and the arsenopyrite/$CoSb_2$ types exhibit lower symmetry, which makes them more susceptible for structural deviations in the calculations.

IV. RESULTS AND DISCUSSION

The energetic aspect of the performed structure optimizations is expressed in stability diagrams in Figure 2 and structural data of the energetically favored structures are given in Table II. In case experimental data is available, the calculated values are in very good agreement with the experimental ones. Thus, the structure predictions for potential new phases are believed to be reasonably accurate. A slight overestimation of lattice constants and distances is common when the GGA functional is used.

Prior to the introduction of the stability diagrams, some energetic considerations have to be made. Absolute energy values of polymorphs can be directly associated with each other. When the atom type or the stoichiometry is changed, a direct comparison of absolute energies becomes impossible. Concerning the atom type, energies of phases with different pnictide atoms can be related to each other with the help of the presented stability diagrams of nickel dipnictides. Trends for the fifth main group can be derived in terms of relative energy differences between the (partly hypothetical) phases. The same is possible for a substitution of the metal atoms, which will be shown elsewhere. The examination of electronic stabilities comes along with an energetic consideration of competing phases with different compositions. As a direct comparison is not feasible, a reference system must be established. For obvious reasons, the reference system is AB_2 (NiPn_2) in this case (in analogy to a realistic scenario of a closed system with an initial sample ratio of Ni:Pn = 1:2). The conversion into an atomic ratio of 1:2 is carried out as a summation of the proportionate energies of different Ni_xPn_y phases or the elements to attain the NiPn_2 stoichiometry. All reported Ni_xPn_y compounds are considered and their energies are calculated for every possible combination with all group 5 elements. The energies of the elements correspond to their most stable modifications α-N_2, orthorhombic (black) P, trigonal (grey) As and Sb, and rhombohedral Bi.

The results of the calculations are merged in the announced stability diagrams (Figure 2). Squares in the diagrams represent the investigated NiPn_2 structure types. The energies of the elements and competing binary phases are symbolized by horizontal "decomposition" lines. Bold dashed-dotted lines (green) represent the sum of the energies of the elements. Solid lines express the energies of the most stable combinations of a *known* Ni_xPn_y phase and an element (bold, blue) or a different *known* Ni_xPn_y phase (thin, black), respectively (yielding a Ni:*Pn* sample ratio of 1:2 in each case). These lines are dashed when the calculated lowest-energy combination contains a hypothetical phase. All NiPn_2 compounds under consideration for *Pn* = P, As, Sb, Bi are

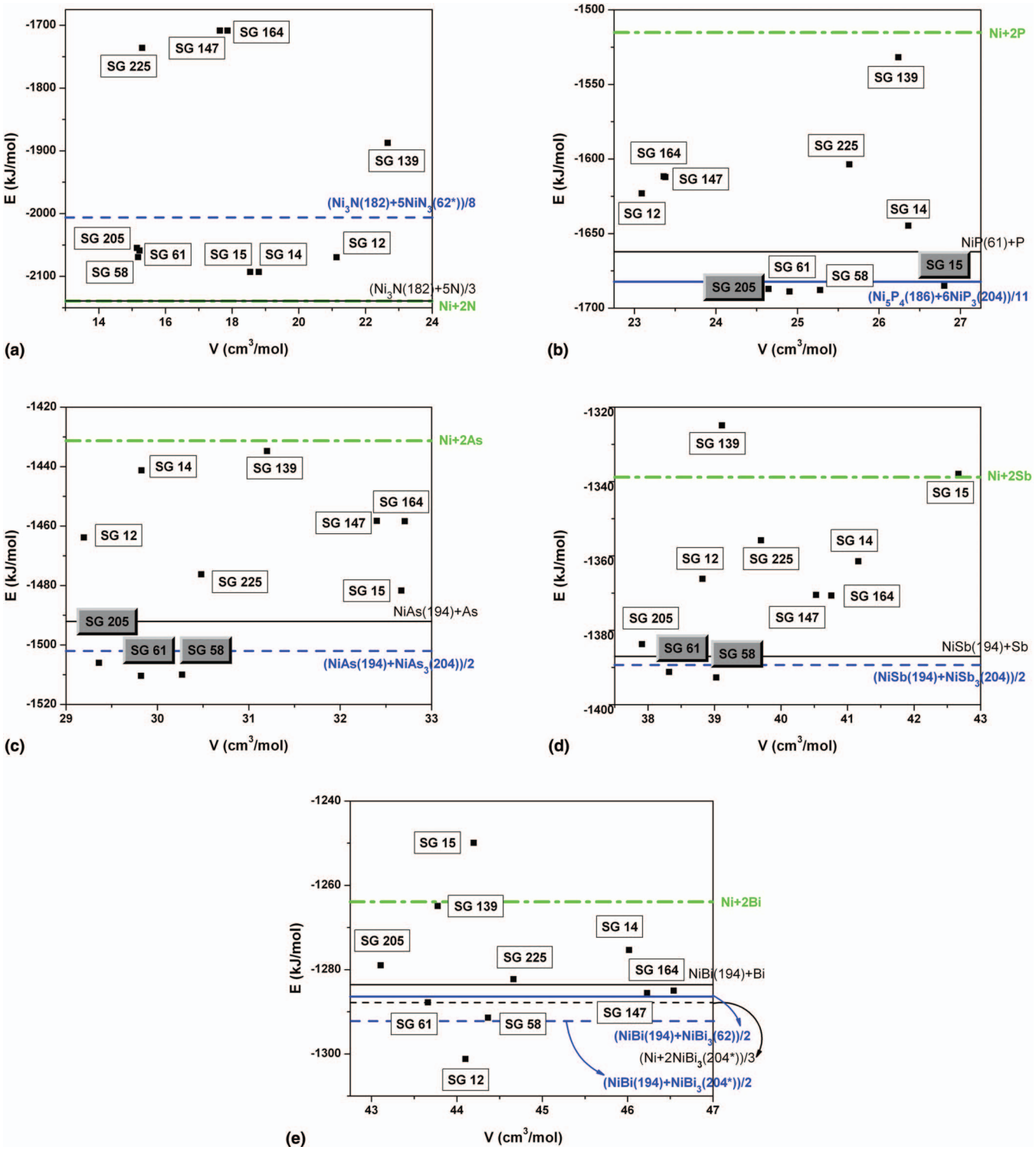

FIG. 2. Stability diagrams of nickel dipnictides from (a) NiN_2, (b) NiP_2, (c) $NiAs_2$ to (d) $NiSb_2$, and (e) $NiBi_2$. Squares represent the investigated MPn_2 structure types, and horizontal "decomposition lines" reflect the energies of competing phases. Bold dashed-dotted lines (green) represent the sum of the energies of the lowest energy polymorphs of the elemental crystals. Solid lines express the energies of the most stable combinations of a Ni_xPn_y phase and an element (bold, blue) or a different Ni_xPn_y phase (thin, black). If a lowest-energy decomposition line involves a hypothetical phase, it is dashed and the related hypothetical space group number is marked with a star. The boxes with the space group numbers corresponding to the investigated MPn_2 structure types are grayed out for experimentally known compounds.

expected to be energetically stable relative to the sum of the energies of their constituent elements (except SG 15 in case of $NiSb_2$ and $NiBi_2$ as well as SG 139 in case of $NiSb_2$).

The stability diagram for Pn = N clearly poses an exceptional position in the pnictide row (Figure 2(a)). All investigated structure types are unstable with respect to decomposition into their elements and Ni_3N (SG $P6_322$ (182)) plus nitrogen (the two lines in the diagram are nearly congruent by coincidence). Some of the structures undergo significant distortions to reach local energetic minima. Remarkably, one of

TABLE II. Calculated structural data of energetically favored structure types. Experimental data are included as reference where available.

Ni*Pn*$_2$	Space group (no.)	Proto-type	*a* (Å)	*b* (Å)	*c* (Å)	*V* (Å^3)	*β* (deg)	*d*(Ni-*Pn*) (Å)	Ø *d*(Ni-*Pn*) (Å)	*d*(*Pn*-*Pn*) (Å)
NiN_2	*Pa*-3 (205)	p-FeS_2	4.65	…	…	100.6	…	2.025 (6x)	2.025	1.275
	Pnnm (58)	m-FeS_2	3.78	4.65	2.87	50.4	…	1.997 (2x) 2.039 (4x)	2.025	1.259
	Pbca (61)	$NiAs_2$	4.71	9.27	4.63	202.3	…	1.994 2.011 (2x) 2.016 2.066 (2x)	2.027	1.266
	*I*4/*mcm* (140)		4.55	…	6.02	62.5	…	1.892 (4x)	1.892	1.233
NiP_2	*Pa*-3 (205)	p-FeS_2	5.47	…	…	163.7	…	2.285 (6x)	2.285	2.196
	Exp[32]		5.4706	…	…	163.72	…	2.293 (6x)	2.293	2.121
	Pnnm (58)	m-FeS_2	4.38	5.49	3.49	84.0		2.254 (2x) 2.284 (4x)	2.274	2.205
	Pbca (61)	$NiAs_2$	5.53	10.93	5.47	330.8	…	2.262 2.266 2.271 2.281 2.285 2.291	2.276	2.206
	*C*2/*c* (15)	KO_2	6.48	5.61	6.15	178.0	127.18	2.205 (4x)	2.205	2.234
	Expt.[36]		6.3660	5.6150	6.0720	175.1	126.22	2.205 (2x) 2.208 (2x)	2.207	2.219
$NiAs_2$	*Pa*-3 (205)	p-FeS_2	5.80	…	…	195.0	…	2.407 (6x)	2.407	2.475
	Expt.[32]		5.7634	…	…	191.44	…	2.399 (6x)	2.399	2.396
	Pnnm (58)	m-FeS_2	4.78	5.84	3.60	100.5	…	2.368 (2x) 2.408 (4x)	2.395	2.499
	Expt.[23]		4.7583	5.7954	3.5449	97.76	…	2.354 (2x) 2.379 (4x)	2.371	2.487
	Pbca (61)	$NiAs_2$	5.90	11.52	5.82	395.8	…	2.375 2.386 2.400 2.402 2.411 2.421	2.399	2.498
	Expt.[24]		5.799	11.407	5.753	380.56	…	2.359 (2x) 2.367 2.376 2.377 2.393	2.372	2.431
	*C*2/*c* (15)	KO_2	6.82	5.99	6.67	108.5	127.16	2.205 (4x)	2.205	2.234
$NiSb_2$	*Pa*-3 (205)	p-FeS_2	6.31	…	…	251.8	…	2.605 (6x)	2.605	2.891
	Pnnm (58)	m-FeS_2	5.23	6.37	3.89	129.8	…	2.558 (2x) 2.597 (4x)	2.584	2.930
	Expt.[25]		5.184	6.318	3.841	125.8	…	2.538 (2x) 2.569 (4x)	2.559	2.883
	Pbca (61)	$NiAs_2$	6.45	12.44	6.34	509.1	…	2.561 2.576 2.586 2.591 2.594 2.632	2.590	2.925
	Expt.[35]		6.3643	12.3670	6.2866	494.8	…	2.533 2.554 2.572 2.573 2.584 2.596	2.569	2.860
$NiBi_2$	*Pa*-3 (205)	p-FeS_2	6.59	…	…	286.3	…	2.712 (6x)	2.712	3.124
	Pnnm (58)	m-FeS_2	5.57	6.68	3.95	147.3	…	2.670 (2x) 2.694 (4x)	2.686	3.157
	Pbca (61)	$NiAs_2$	6.75	12.92	6.65	580.0	…	2.672 2.686 2.689 2.702 2.710 2.723	2.697	3.157
	*C*2/m (12)	CrP_2	13.07	4.10	5.56	292.91	100.9	2.754 (2x) 2.763 (2x) 2.780 2.908 2.927	2.807	Ø3.565 (7x)

these distorted structures is the global minimum in the NiN_2 stability diagram. Whereas the experimentally found lowest-energy form of homologous PtN_2 is the pyrite type,[20] NiN_2 seems to prefer a different structure. It is reached by a full geometry optimization of both the arsenopyrite/$CoSb_2$ and the KO_2 type structures (Figure 3). The structure is tetragonal with space group *I*4/*mcm* (140) and related to the SrS_2 type,[65] which crystallizes in the same space group. In contrast to alternating planes of Sr and S_2 entities, the respective planes in our calculated structure are relocated into each other. This particular structure is attributed to the valences and bonding states in NiN_2. The calculated N-N distance of 1.23 Å indicates a double bond diazenide ion as found in Ref. 66. It is remarkably shorter than the N-N single bonds (1.42 Å for $[N_2]^{4-}$) that occurs in PtN_2. Thus, Ni^{2+} prefers a planar coordination in NiN_2.

The other dumbbell-like structure types are relatively low in energy with the marcasite type slightly preferred over the pyrite and the $NiAs_2$ type. An almost identical relative cell volume for these phases can be observed as the nitrogen atoms are very small compared to the nickel atoms and thus the metal packing determines the cell size. Due to the exceptional size and bonding behavior of nitrogen, some of the layered structures are significantly distorted. This applies particularly for the hypothetical $PdBi_2$-type phases (SG 12 and SG 139) where the original structures are rearranged to layers with inter- (SG 12) and intra-layer (SG 139) nitrogen dumbbells (cf. the CaC_2 structure type). $PtBi_2$-type NiN_2 (SG 147) is reassembled to its CdI_2 aristotype (SG 164), which is apparent throughout the pnictide row. Along with the fluorite type (SG 225), the CdI_2 type is remarkably energetically disfavored. In contrast, the occurrence of N_2 units in the optimized $PdBi_2$-type phases makes them relatively stable. The synthesis of a NiN_2 compound would certainly require extreme conditions to overcome the energy barrier and such a compound would most likely contain N-N entities. Although facing instability with respect to its constituent elements, a possible synthesis is indicated when looking at the homologous Pd and Pt dipnictides which were calculated as metastable.

In the remaining stability diagrams for *Pn* = P, As, Sb, and Bi (Figures 3(b)–3(e)), almost all structures are stable with respect to decomposition into their elements, and structural deformations become less numerous and distinctive. Dumbbell-like structures are still energetically favored and their relative volume ratios stay fairly proportional aside from the arsenopyrite/$CoSb_2$ type (SG 14). As explained above, the arsenopyrite/$CoSb_2$ type is a derivative of the marcasite type (SG 58) with minor structural distortions. Depending on the exact structural input for the calculations, the arsenopyrite/$CoSb_2$ type either adapts the marcasite structure or it is subject to structural deformations. These deformations (rising from NiP_2 to $NiBi_2$) lead to the development of three-dimensional networks with cavities that explain the relative volume increase. The arsenopyrite/$CoSb_2$ type is the only dumbbell-like structure type among the present selection that has not been reported for any Ni*Pn*$_2$ compound and the existence of such a compound seems to be unlikely according to our calculations (i.e., the structural deformations that

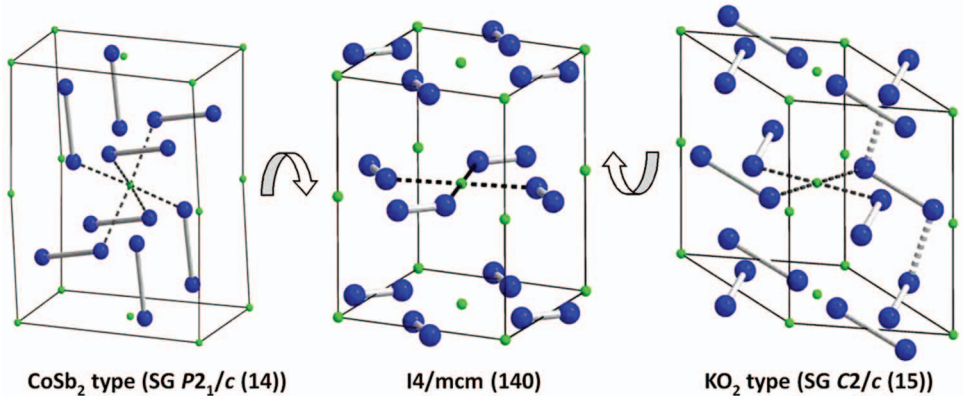

FIG. 3. The crystal structure of the calculated lowest-energy structure candidate of NiN_2 (SG *I*4/*mcm* (140)) (middle) and related structural fragments of its parent structures SG $P2_1/c$ (14) (left) and SG *C*2/*c* (15) (right), respectively. The fragments are meant to indicate structural similarities and do not represent the unit cells in a different setting. Small (green) spheres represent Ni, large (blue) spheres represent N.

lead from the marcasite to the arsenopyrite/$CoSb_2$ type do not cause a gain in energy for the investigated systems). The other structure types with *Pn*-*Pn* dimers (pyrite (SG 205), marcasite (SG 58), and $NiAs_2$ type (SG 61)) show very similar behaviors concerning energy and volume in all stability diagrams, as expected, because of the described structural relationships. For NiP_2 (Figure 2(b)), they are located in the same energy range along with KO_2-type NiP_2, which is the experimentally determined stable phase at ambient conditions. Moreover, these compounds are situated below the decomposition lines. Whereas pyrite-type NiP_2 has been discovered as a high temperature phase, marcasite- and $NiAs_2$-type NiP_2 are hitherto unknown and come into consideration as further polymorphs based on our calculations. Accurately defined reaction conditions are probably necessary to get there as the energy differences are just a few kJ/mol.

As a remark on the decomposition lines in the NiP_2 diagram, we want to underline the importance of the consideration of concurring phases with different atomic constitutions in all possible combinations. The summation of the energies of these combinations must correspond to the desired atomic ratio (cf. sample ratios for experimentalists in a solid state reaction) in order to make statements about phase stabilities. The lowest-energy combination (Ni:P = 1:2) for a binary phase with phosphorus exists for NiP (SG *Pbca* (61)), the lowest-energy combination for two binary phases exists for Ni_5P_4 (SG $P6_3mc$ (186)) and NiP_3 (SG *Im*-3 (204)) (see Figure 2(b)). *Per se*, the formation energy for Ni_5P_4 is slightly lower than for NiP (4.45 kJ/mol) and distinctly lower than for NiP_3 (17.83 kJ/mol). The formation energies of all compounds are explicitly negative (–50.28 kJ/mol-atom, −45.83 kJ/mol-atom, and −32.46 kJ/mol-atom). To get to the desired stoichiometry of Ni:P = 1:2, relatively more (energetically significantly unfavorable) P is required in case of Ni_5P_4 and the combination with NiP is more stable. However, the combination with energetically less unfavorable NiP_3 and the relatively smaller amount of NiP_3 that is needed to get to the 1:2 ratio leads to a preference of Ni_5P_4. A consideration of all possible combinations is always necessary to obtain reliable stability predictions.

Another hint for the existence of the mentioned potential new NiP_2 phases is given by looking at the polymorphism and the stability diagram of $NiAs_2$ (Figure 2(c)). Again, the dumbbell-like structure types are in the same energy range below the decomposition lines and they have all been experimentally identified as polymorphs of $NiAs_2$. Other phases like KO_2-type $NiAs_2$ seem to be rather unlikely in face of the considerable energy differences and the position above the decomposition lines. For the stability diagrams of $NiAs_2$ and $NiSb_2$, these lines consist of Ni*Pn* (NiAs type, SG $P6_3/mmc$ (194)) plus *Pn* and Ni*Pn* plus hypothetical $NiPn_3$ (SG *Im*-3 (204)), respectively. In contrast to $NiAs_2$, pyrite type $NiSb_2$ is situated above the decomposition lines and it has not been prepared up to now (Figure 2(d)). The existing dumbbell-like polymorphs of $NiAs_2$, on the other hand, are located below the decomposition lines. Extreme conditions will be necessary to overcome the energy barrier in order to attain a pyrite type $NiSb_2$ phase. In this context, an already slightly indicated trend becomes more obvious. Among the dumbbell-like structures, the pyrite type gets less and the marcasite type more stable towards higher pnictide homologues (see also $NiBi_2$ (Figure 2(e))). Increasing interactions between dipnictide units are supposably more or less energetically favorable for the different structure types. All other structure types in the discussed stability diagrams seem to be out of reach for synthesis, but this definitely changes for $NiBi_2$.

Whereas dumbbell-like structures are unambiguously preferred in the NiN_2 landscape, the gap vanishes with increasing atomic masses of the pnictides. Nevertheless, the preparation of structures without dumbbells seems to be very unlikely for *Pn* = P, As, and Sb. Only for the $NiBi_2$ landscape, they play an important role in energetic considerations where all investigated structure types range in a similar energy region. No $NiBi_2$ compound is known from the literature and there is one particular structure type that is clearly located in the global minimum of the stability diagram: the froodite type (SG 12) which belongs to the corresponding $PdBi_2$ homologue. It is stable with respect to decomposition for all combinations, which implicates a high potential for a successful synthesis of this compound. The lowest-energy

decomposition lines contain hypothetical $NiBi_3$ (SG *Im*-3 (204)), and froodite type $NiBi_2$ is the only phase that is clearly located below them. If hypothetical phases remain disregarded, the marcasite (58) and the pararammelbergite (61) type should also be taken into consideration as they are located below the decomposition lines of NiBi (NiAs type, SG $P6_3/mmc$ (194)) plus Bi and NiBi plus $NiBi_3$ ($RhBi_3$ type, SG *Pnma* (62)). It should be emphasized here that pararammelsbergite (61) type $PtBi_2$ has actually been synthesized.[46]

On looking at the volumes of the non dumbbell-like structures, especially the fluorite type (SG 225), they turned out to be a very appropriate reference compound for the whole dipnictide row, with constant relative volume and continuously decreasing relative energy. The same applies for the CdI_2 type except for the case of NiP_2 where a significant volume contraction is caused by strong P-P interactions between the layers. The $PdBi_2$-related structure types froodite (SG 12) and urvantsevite (SG 139) follow opposite trends of relative volume expansion (SG 12) and contraction (SG 139). From NiP_2 to $NiBi_2$, sort of interlocked layers are loosened for the first and intralayer pnictide-pnictide interactions become stronger for the latter.

The stability diagrams should provide a basis for a simple estimation of phase stabilities of certain systems. This allows for the derivation of significant information like trends within the periodic table or the indication of potential new phases. For an even more accurate treatment of the systems especially at high pressures and high temperatures, more extensive calculations have to be performed. Particularly with energy differences of just a few kJ, only slightly changed energy values can lead to inversions of the (relative) stabilities.

V. CONCLUSION

By means of the presented stability diagrams, a straightforward graphical representation of (relative) phase stabilities based on DFT calculations was presented for compounds with polyanionic fragments. Nickel dipnictides proved to be an ideal model system with the combination of a reference basis in terms of reported polymorphism and unexplored room for the discovery of new phases. Experimental data were correctly reflected in all stability diagrams and hints for the existence of new (possibly metastable) phases can be drawn from the diagrams. In this context, decomposition lines proved themselves as reliable tool for the estimation of experimental accessibility under moderate conditions. The crystal structures of the determined low-energy structures were offered in detail. Relationships between the existing $NiPn_2$ phases were shown using structural fragments corresponding to the marcasite structure type.

Suitable structure candidates for the optimizations were chosen among the experimentally reported and closely related structure types along with selected reference compounds. This set of structure types was systematically optimized for the chemical series of nickel dipnictides. Starting with the archetype structures, full optimizations were performed with a conjugate gradient algorithm. As a matter of fact, this common way of creating the input for the calculations involves the possibility that different structure types are overlooked. However, the example of NiN_2 proves that new structure types can be discovered during the geometry optimization. A main goal was the derivation of energetic trends for the selected set of structure types within the periodic table. These trends and structural preferences for the investigated nickel dipnictides could be successfully derived from the stability diagrams. The consideration of competing phases (with different stoichiometry) turned out to be crucial for the investigated systems since many of the hypothetical phases are stable with respect to their constituent elements but not with respect to certain combinations of competing phases (and elements). All in all, the presented method is suitable for further systematic investigations of related systems (starting with the substitution of Ni by Pd and Pt).

Taking another step further, an expansion to completely different systems and the incorporation of thermodynamics and high pressure is aspired. Indeed, the calculation of the electronic ground state gives clear hints at the stabilities of the investigated systems and the conclusions drawn from the stability diagrams are expected to be valid also for the application of moderate pressure and temperature. Nevertheless, the evolution of the stability diagrams at high pressure and high temperature with a focus on the development of relative stabilities is subject to further investigations. This allows for an evaluation of the scope of the present results and the derivation of additional trends within the periodic table.

ACKNOWLEDGMENTS

The authors would like to thank the Deutsche Forschungsgemeinschaft (DFG, SPP1415, WE 4284/3-2) and the German Academic Exchange Service (DAAD) for financial support.

[1] G. J. Snyder and E. S. Toberer, Nature Mater. **7**, 105 (2008).
[2] T. Nilges, O. Osters, M. Bawohl, J. L. Bobet, B. Chevalier, R. Decourt, and R. Weihrich, Chem. Mater. **22**, 2946 (2010).
[3] M. Jansen, Angew. Chem., Int. Ed. **41**, 3746 (2002).
[4] A. R. Oganov and C. W. Glass, J. Chem. Phys. **124**, 244704 (2006).
[5] R. P. Stoffel, C. Wessel, M. W. Lumey, and R. Dronskowski, Angew. Chem., Int Ed. **49**, 5242 (2010).
[6] M. Wessel and R. Dronskowski, J. Am. Chem. Soc. **132**, 2421 (2010).
[7] O. Osters, T. Nilges, F. Bachhuber, F. Pielnhofer, R. Weihrich, M. Schoneich, and P. Schmidt, Angew. Chem., Int. Ed. **51**, 2994 (2012).
[8] X. W. Zhang, L. P. Yu, A. Zakutayev, and A. Zunger, Adv. Funct. Mater. **22**, 1425 (2012).
[9] R. Weihrich, S. F. Matar, E. Betranhandy, and V. Eyert, Solid State Sci. **5**, 701 (2003).
[10] R. Weihrich, V. Eyert and S. F. Matar, Chem. Phys. Lett. **373**, 636 (2003).
[11] R. Weihrich, D. Kurowski, A. C. Stuckl, S. F. Matar, F. Rau, and T. Bernert, J. Solid State Chem. **177**, 2591 (2004).
[12] M. Meier and R. Weihrich, Chem. Phys. Lett. **461**, 38 (2008).
[13] F. Bachhuber, J. Rothballer, F. Pielnhofer and R. Weihrich, Z. Anorg. Allg. Chem. **636**, 2043 (2010).
[14] F. Bachhuber, J. Rothballer, F. Pielnhofer, and R. Weihrich, J. Chem. Phys. **135**, 124508 (2011).
[15] F. Bachhuber, J. Rothballer, T. Söhnel, and R. Weihrich, Z. Anorg. Allg. Chem. **638**, 1612 (2012).
[16] G. Bergerhoff and I. D. Brown, *Crystallographic Databases* (International Union of Crystallography, Chester, 1987).
[17] A. Belsky, M. Hellenbrandt, V. L. Karen, and P. Luksch, Acta Crystallogr., Sect. B: Struct. Sci. **58**, 364 (2002).
[18] V. Eyert, K. H. Hock, S. Fiechter, and H. Tributsch, Phys. Rev. B **57**, 6350 (1998).
[19] I. Opahle, K. Koepernik, and H. Eschrig, Phys. Rev. B **60**, 14035 (1999).

[20]J. von Appen, M. W. Lumey, and R. Dronskowski, Angew. Chem., Int. Ed. **45**, 4365 (2006).
[21]C. Villevieille, C. M. Ionica-Bousquet, J. C. Jumas, and L. Monconduit, Hyperfine Interact. **187**, 71 (2008).
[22]W. N. Stassen and R. D. Heyding, Can. J. Chem. **46**, 2159 (1968).
[23]H. Holseth and A. Kjekshus, Acta Chem. Scand. **22**, 3273 (1968).
[24]M. E. Fleet, Am. Mineral. **57**, 1 (1972).
[25]A. Kjekshus, P. G. Peterzens, T. Rakke, and A. F. Andresen, Acta Chem. Scand. **33a**, 469 (1979).
[26]S. Kaiman, *Geological Series 51* (University of Toronto Studies, 1947), p. 49.
[27]S. L. Bennett and R. D. Heyding, Can. J. Chem. **44**, 3017 (1966).
[28]H. Holseth and A. Kjekshus, Acta Chem. Scand. **22**, 3284 (1968).
[29]A. Kjekshus, T. Rakke, and A. F. Andresen, Acta Chem. Scand. **28a**, 996 (1974).
[30]A. Kjekshus and T. Rakke, Acta Chem. Scand. **31a**, 517 (1977).
[31]R. A. Munson, Inorg. Chem. **7**, 389 (1968).
[32]P. C. Donohue, T. A. Bither, and H. S. Young, Inorg. Chem. **7**, 998 (1968).
[33]M. Rosenqvist, Acta Metall. **1**, 761 (1953).
[34]H. Holseth, A. Kjekshus, and A. F. Andresen, Acta Chem. Scand. **24**, 3309 (1970).
[35]H. Takizawa, K. Uheda, and T. Endo, Intermetallics **8**, 1399 (2000).
[36]E. Larsson, Ark. Kemi **23**, 335 (1965).
[37]S. V. Orishchin, V. S. Babizhetskii, and Y. B. Kuz'ma, Crystallogr. Rep. **45**, 894 (2000).
[38]E. Gregoryanz, C. Sanloup, M. Somayazulu, J. Badro, G. Fiquet, H. K. Mao, and R. J. Hemley, Nature Mater. **3**, 294 (2004).
[39]J. C. Crowhurst, A. F. Goncharov, B. Sadigh, C. L. Evans, P. G. Morrall, J. L. Ferreira, and A. J. Nelson, Science **311**, 1275 (2006).
[40]J. C. Crowhurst, A. F. Goncharov, B. Sadigh, J. M. Zaug, D. Aberg, Y. Meng, and V. B. Prakapenka, J. Mater. Res. **23**, 1 (2008).
[41]N. N. Zharavlev, Can. Mineral. **11**, 903 (1973).
[42]H. J. Wallbaum, Z Metallkd **35**, 200 (1943).
[43]N. N. Zhuravlev and A. A. Stepanova, Sov. Phys., Crystallogr. **7**, 241 (1962).
[44]S. Furuseth, K. Selte, and A. Kjekshus, Acta Chem. Scand. **19**, 735 (1965).
[45]T. Biswas and K. Schubert, J. Less-Common Met. **19**, 223 (1969).
[46]Y. C. Bhatt and K. Schubert, Z. Metallkd. **71**, 581 (1980).
[47]N. E. Brese and H. G. Vonschnering, Z. Anorg. Allg. Chem. **620**, 393 (1994).
[48]A. F. Young, C. Sanloup, E. Gregoryanz, S. Scandolo, R. J. Hemley, and H. K. Mao, Phys. Rev. Lett. **96**, 155501 (2006).
[49]J. Ren, J. Wang, and J. Li, J. Fuel Chem. Tech. **35**, 458 (2007).
[50]D. D. Zhao, L. C. Zhou, Y. Du, A. J. Wang, Y. B. Peng, Y. Kong, C. S. Sha, Y. F. Ouyang, and W. Q. Zhang, CALPHAD: Comput. Coupling Phase Diagrams Thermochem. **35**, 284 (2011).
[51]Z. W. Chen, X. J. Guo, Z. Y. Liu, M. Z. Ma, Q. Jing, G. Li, X. Y. Zhang, L. X. Li, Q. Wang, Y. J. Tian, and R. P. Liu, Phys. Rev. B **75**, 054103 (2007).
[52]W. Chen, J. S. Tse, and J. Z. Jiang, Solid State Commun. **150**, 181 (2010).
[53]H. R. Soni, S. D. Gupta, S. K. Gupta, and P. K. Jha, Physica B **406**, 2143 (2011).
[54]J. P. Perdew, K. Burke, and M. Ernzerhof, Phys. Rev. Lett. **77**, 3865 (1996).
[55]J. P. Perdew, K. Burke, and M. Ernzerhof, Phys. Rev. Lett. **78**, 1396 (1997).
[56]G. Kresse, J. Non-Cryst. Solids **192–193**, 222 (1995).
[57]G. Kresse and J. Hafner, Phys. Rev. B **49**, 14251 (1994).
[58]G. Kresse and J. Furthmuller, Comput. Mater. Sci. **6**, 15 (1996).
[59]G. Kresse and J. Furthmuller, Phys. Rev. B **54**, 11169 (1996).
[60]P. E. Blochl, Phys. Rev. B **50**, 17953 (1994).
[61]G. Kresse and D. Joubert, Phys. Rev. B **59**, 1758 (1999).
[62]G. Brostigen and A. Kjekshus, Acta Chem. Scand. **24**, 2983 (1970).
[63]G. Brostigen and A. Kjekshus, Acta Chem. Scand. **24**, 2993 (1970).
[64]A. Kjekshus and T. Rakke, Struct. Bonding (Berlin) **19**, 85 (1974).
[65]H. G. von Schnering and N. K. Goh, Naturwiss. **61**, 272 (1974).
[66]G. V. Vajenine, G. Auffermann, Y. Prots, W. Schnelle, R. K. Kremer, A. Simon, and R. Kniep, Inorg. Chem. **40**, 4866 (2001).